Early warning indicators of war and peace through the landscapes and flux quantifications

Linqi Wang [1,2] Kun Zhang,[2] and Jin Wang [3,*]

[1]*Center of Theoretical Physics, College of Physics, Jilin University, Changchun 130012, China*

[2]*State Key Laboratory of Electroanalytical Chemistry, Changchun Institute of Applied Chemistry, Chinese Academy of Sciences, Changchun 130022, China*

[3]*Department of Chemistry and Department of Physics and Astronomy, State University of New York at Stony Brook, Stony Brook, New York 11794, USA*

(Received 30 October 2023; accepted 6 February 2024; published 21 March 2024)

War and peace, spanning history, deeply affect society, economy, and individuals. Grasping their dynamics is vital to lessen harm and foster global peace. Yet, quantifying them remains hard. Our goal is to create a simple qualitative model using landscape and flux theory, exploring war and peace mechanisms. In this symmetric network, they appear as separate attraction basins, dynamically shifting. Analyzing landscape shape gives insights into global stability. Near critical points, indicators like cross correlations, autocorrelation times, and flickering frequency surge, as warnings. We also calculate the irreversible path between war and peace due to rotational flux. Global sensitivity analysis identifies history's role in system stability. In summary, our research unveils a way to understand war and peace complexities, enhancing knowledge of key elements that lead to conflict, aiding resolution.

DOI: 10.1103/PhysRevE.109.034311

I. INTRODUCTION

Peace and war are universal social phenomena. Peace represents the ideal environment that people aspire to, while war signifies a state of violent conflict that is undesirable. The occurrence of a war is influenced by various factors, including political, economic, military, scientific, technological, and natural conditions. These factors, together with human agency, contribute to the development and outcome of the war. Human society, as the natural world, experiences both harmonious aspects and disharmonious aspects. Peace and war, two fundamental and conflicting phenomena, coexist within human societies. This prompts us to inquire about the key factors that contribute to the emergence of the war and the factors that foster peace. When people talk about peace, they think of no war, no violent conflict—this is only a negative peace that cannot effectively prevent the appearance of violence and conflict. To understand the drivers of peace, it is essential to go beyond a mere absence of war, and studies have explored the mechanisms of war and conflict [1]. Dynamic system theory has found applications in various social phenomena and provides a conceptual framework for understanding and resolving conflicts [2–5]. Peace or war is essentially a dynamic process. Conflicts arise from the complex interactions of multiple factors, and understanding the intricate details of these interactions sheds light on the origins of conflicts [6–8]. These factors do not operate in isolation but rather form an interconnected complex network. The real world hosts a variety of networks, such as social networks, information networks, technical networks, and biological networks, each characterized by distinct structures and functions [9]. By looking at war and peace from a nonlinear dynamic perspective, we synthesize the factors that affect the peace in a system. The researchers propose that the causal loop diagram of the peace system forms a type of network. It enables qualitative determination of complex peace factors and their relationships [10]. Mathematical models based on differential equations offer a quantitative approach, allowing us to understand the system's behavior, properties, and its dynamics towards war or peace [11–13]. By solving these differential equations, we can gain insight into the factors that influence the system's trajectory towards war or peace, including the factors with the greatest impact. Such deterministic models offer realistic predictions and enable policy interventions as well as possible and early warning of the potential turbulence based on the system's overall evolutionary trend. The topology of the causal network determines the ultimate fate of the system, reflecting whether the world or region we inhabit is at war or peace through attractors.

Current models describing the evolution of sustainable peace systems primarily operate in a deterministic manner. However, in reality, dynamic processes are subject to inevitable noise [14]. Therefore, a more realistic model should consider both intrinsic and extrinsic fluctuations. Furthermore, the system of the study is often an open one as living systems and chemical reaction systems. It exchanges information, energy, and matter with the external environment. Therefore, the system is usually in nonequilibrium. Landscape and flux theory for non-equilibrium systems has been applied to various disciplines, including protein folding, biomolecule recognition, evolution of biological systems, cell cycle, differentiation and development, cancer, neural networks, brain function, and cross-scale research on genome structure dynamics [15,16].

*jin.wang.1@stonybrook.edu

In this paper, we revise the existing peace model based on landscape and flux theory and develop a comprehensive nonequilibrium dynamical model for war and peace. Through quantitative analysis using landscape and flux theory, war and peace are described as two attractor basins. We will illustrate the switching dynamics between war and peace through the height of the barrier and the escape time determined by it. We explore the nonequilibrium dynamics and thermodynamics of the war and peace network, which were not considered in previous sustainable peace models to the best of our knowledge. We find that the rotational flux serves as the dynamical source for bifurcations while the entropy production rate (EPR), which describes the thermodynamic cost, serves as the thermodynamic source for the nonequilibrium phase transition of the war and peace system, while the rotational flux acts as the dynamical bifurcation source. In our paper, we compare and analyze the three early warning indicators average flux, entropy production, and time irreversibility for predicting critical points. Compared to the traditional critical slowing down prediction, we find that the time irreversibility of the cross-correlation functions can serve as the signals for critical transitions between alternative stable states caused by the existence of rotational flux. This provides an early warning indication for the nonequilibrium system approaching the critical bifurcation point, usually preceding the traditional critical slowing down prediction, while the flickering frequency is the latest signal. Furthermore, we will explore the nonequilibrium dynamical path of war and peace and conduct a global sensitivity analysis on various parameters in the model to identify key influencing factors on war and peace.

II. MODEL

Over the past few years, an interdisciplinary team of scientists, academics, policymakers, and practitioners brought together by the Advanced Consortium on Cooperation, Conflict, and Complexity (AC4), has made significant strides in advancing our understanding of sustainable peace and its intricate dynamics [11,13,17]. However, when it comes to the nonequilibrium aspect, the quantification of war and peace still poses significant challenges. In this paper, we primarily consider six variables that impact peace: positive future expectations, positive reciprocity, positive history memory, negative history memory, negative reciprocity, and negative future expectations. Figure 1 shows a causal loop diagram comprising these six factors, with positive and negative factors interconnected to form a causal network. Previous studies have employed differential equation models based on dynamical systems theory, with each factor governed by the following equation [12]:

$$\frac{dx_i}{dt} = -|m_i|x_i + b_i + \sum_{j=1}^{n} c_{ij}\tanh(x_j). \tag{1}$$

Here, x_i (for $i = 1, 2, ..., 6$) represents the peace impact factor, and we limit these six variables to $x_i \geqslant 0$ to ensure that a negative peace factor, acting through a negative link, does not produce a positive effect [13]. The first term on the left side represents the first derivative in time of each peace factor, and m_i is the constant of the exponential decay term,

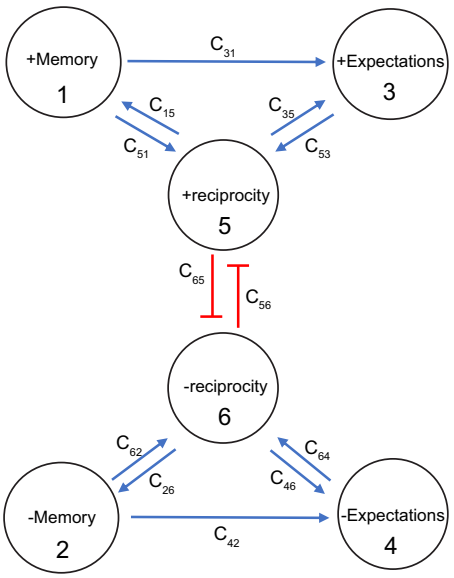

FIG. 1. Causal loop diagrams. The arrow lines represent the interrelation between the factors, red lines represents mutual inhibition of factors, blue lines represents mutual promotion.

reflecting the self degradation or system's degree of memory. This term is introduced to prevent unbounded growth of each variable. In other words, factors cannot indefinitely influence the system. The second term b_i represents the self-reinforcing term of each factor. The third term describes the interconnection between the factors, where c_{ij} denotes the strength of the influence from variable j to i. This parameter is crucial in transforming the qualitative causal loop diagram into a quantitative model [18]. The nonlinear hyperbolic tangent function $\tanh(x)$ ensures that each variable has a nearly linear influence on other variables when its value is very low, and reaches a maximum impact threshold when the value of each variable is extremely high. The graph of the hyperbolic tangent function is shown in Fig. 2.

Although Eq. (1) has been employed in previous research on sustainable peace and its complexity [13], a comprehensive quantitative characterization of peace and war at the nonequilibrium level is still lacking. Equation (1) is mathematically a system of deterministic dynamical ordinary differential equations. However, in practice, the system is always subject to noise. Thus, we incorporate the fluctuations of each factor and construct a stochastic model. Since negative variables

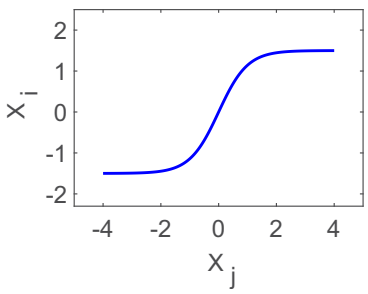

FIG. 2. Two factors have a relationship expressed as $x_i = c_{ij}\tanh(x_j)$, where $c_{ij} = 1.5$.

TABLE I. The strength of the influence.

Symbol	Interpretation
C_{15}	The strength of the influence of the positive reciprocity on the positive history memory
C_{26}	The strength of the influence of the negative reciprocity on the negative history memory
C_{31}	The strength of the influence of the positive history memory on the positive expectations
C_{35}	The strength of the influence of the positive reciprocity on the positive expectations
C_{42}	The strength of the influence of the negative history memory on the negative expectations
C_{46}	The strength of the influence of the negative reciprocity on the negative expectations
C_{51}	The strength of the influence of the positive history memory on the positive reciprocity
C_{53}	The strength of the influence of the positive expectations on the positive reciprocity
C_{56}	The strength of the influence of the negative reciprocity on the positive reciprocity
C_{62}	The strength of the influence of the negative history memory on the negative reciprocity
C_{64}	The strength of the influence of the negative expectations on the negative reciprocity
C_{65}	The strength of the influence of the positive reciprocity on the negative reciprocity

have a stronger impact than positive variables [4], the original core engine model with fewer variables tends to push the system towards a state of war. Previous model studies have demonstrated that social peace is the collective outcome of numerous positive factors [18]. However, in this paper, we reconstruct a model encompassing both peace and war by adjusting the strength of the interplay between factors. We aim to explore the underlying mechanism of war and peace within the framework of nonequilibrium landscape and flux theory.

Additionally, our goal is to establish a straightforward and quantitative comprehension of the intricate dynamics governing war and peace. Although our model may appear simplistic, incorporating only six factors, the obtained results demonstrate remarkable consistency with the empirical realities, thereby substantiating the model's robustness and reliability. In this model, the six peace factors satisfy the following equations:

$$\begin{aligned}
\frac{dx_1}{dt} &= -|m_1|x_1 + b_1 + C_{15}\tanh(x_5) + \sqrt{2D}\eta(t),\\
\frac{dx_2}{dt} &= -|m_2|x_2 + b_2 + C_{26}\tanh(x_6) + \sqrt{2D}\eta(t),\\
\frac{dx_3}{dt} &= -|m_3|x_3 + b_3 + C_{31}\tanh(x_1) + C_{35}\tanh(x_5)\\
&\quad + \sqrt{2D}\eta(t),\\
\frac{dx_4}{dt} &= -|m_4|x_4 + b_4 + C_{42}\tanh(x_2) + C_{46}\tanh(x_6)\\
&\quad + \sqrt{2D}\eta(t),\\
\frac{dx_5}{dt} &= -|m_5|x_5 + b_5 + C_{51}\tanh(x_1) + C_{53}\tanh(x_3)\\
&\quad + C_{56}\tanh(x_6) + \sqrt{2D}\eta(t),\\
\frac{dx_6}{dt} &= -|m_6|x_6 + b_6 + C_{62}\tanh(x_2) + C_{64}\tanh(x_4)\\
&\quad + C_{65}\tanh(x_5) + \sqrt{2D}\eta(t). \qquad (2)
\end{aligned}$$

Figure 1 shows three primary types of variables, with each category encompassing both positive and negative influences or characteristics, representing both adverse and favorable aspects within each variable type. Here, factor 1 represents positive history memory, while factor 2 represents negative history memory. Factor 3 represents positive future expectations, and factor 4 represents negative future expectations. Finally, factor 5 represents positive reciprocity, and factor 6 represents negative reciprocity.

Reciprocity refers to the positive or negative influencing behaviors between groups. When members of one group positively influence members of another group, the latter reciprocate with approximately equal or more positive influence. Conversely, if members of one group engage in negative influencing behaviors toward members of another group, it leads to a tit-for-tat negative reciprocity between the groups. Expectations refer to the positive or negative plans, visions, agreements, and aspirations of the groups. History memory specifically includes positive or negative stories, symbols, memories, documents, etc. [17].

In Table I, we give the mutual influence strength of each factor in Eq. (2). Below, we provide a more detailed explanation of the interaction parameters (strength of influence) in the model. C_{51} specifically refers to how much positive historical memory within a group translates into positive reciprocity. For example, if a member of a group has positive historical memories, they are more likely to engage in positive behaviors (reciprocity). Conversely, C_{15} specifically indicates that the more positive reciprocity exists between groups, the more it promotes the formation of positive historical memories between them. On the other hand, C_{62} indicates that past negative historical memories between groups influence and promote the formation of negative reciprocity between them, while C_{26} indicates that negative reciprocity reciprocates with a roughly equal influence on negative historical memories. C_{31} indicates that positive historical memories proportionally translate into positive future expectations, while future expectations do not affect past history. C_{42} indicates that negative historical memories proportionally translate into negative future expectations. C_{35} indicates that positive reciprocity proportionally translates into positive expectations within a group, while C_{53} indicates that positive expectations within a group, in turn, promote more positive reciprocity between groups. C_{46} indicates that negative reciprocity proportionally translates into negative expectations within a group, while C_{64} indicates that negative expectations within a group, in turn, promote more

negative reciprocity between groups. C_{56} indicates that for the more negative reciprocity the corresponding effect will be a decrease in the quantity of positive reciprocity. Conversely, C_{65} indicates that an increase in the quantity of positive reciprocity leads to a decrease in the quantity of negative reciprocity.

In our model, we set all self-reinforcing terms b_i to 0, all exponential factors m_i to -0.9, $C_{15} = C_{26} = C_{31} = C_{42} = C_{51} = C_{62} = 1.5$, $C_{35} = C_{46} = C_{53} = C_{64} = 0.3$, and $C_{56} = C_{65} = -1.5$.

III. METHODS

A. The landscape and flux theory of nonequilibrium system

The stochastic dynamics of nonequilibrium dynamical systems are determined by the landscape and flux that emerge from the interactions in the state space. In our paper, we utilize landscape and flux theory to revise the original six-factor core engine model [12]. In this constructed stochastic dynamics model, the dynamics of these peace factors are governed by the Langevin's equation [19,20]:

$$\frac{dx_i}{dt} = F_i(x_1 ... x_i) + \eta(t). \tag{3}$$

The first term on the left-hand side of the equation represents the time derivative of each peace factor variable. The second term on the right-hand side corresponds to the deterministic force, which is consistent with the term on the right-hand side of the Eq. (2). The third term on the right-hand side of the equation represents the stochastic forces. We consider white Gaussian noise, which exhibits a first-order correlation given by $\langle \eta(t)\eta(t')\rangle = D\delta(t - t')$, where D generally represents a diffusion tensor or diffusion matrix that characterizes the magnitude of the fluctuations. In this case, we assume isotropic noise and treat it as a constant. Due to the influence of noise, the trajectory of each factor becomes uncertain. However, the dynamic behavior or pattern of the system can still be characterized by the probability distribution of its state. At the stochastic level, the probability distribution satisfies the Fokker-Planck equation [21]:

$$\frac{\partial P(x_1, x_2, ...x_i, t)}{\partial t} = -\sum_{i=1}^{n} \frac{[F_i(x_1 ...x_i)\partial P(x_1, x_2, ...x_i, t)]}{\partial x_i} + D \sum_{i=1,j=1}^{n,n} \frac{\partial^2 P(x_1, x_2, ...x_i, t)}{\partial x_i \partial x_j}. \tag{4}$$

The Fokker-Planck equation can be expressed in the form of the conservation laws as $\frac{\partial P}{\partial t} + \nabla \cdot \boldsymbol{J} = 0$. The first term in the equation represents the time derivative of the probability distribution function of the peace system. The second term corresponds to the divergence of the flux. Thus, the change of the probability is equal to the net flux in or out. The probability flux, denoted as $\boldsymbol{J}$, is defined as $\boldsymbol{J} = \boldsymbol{F}P - D\nabla P$, where $\boldsymbol{F}$ represents the driving force of the system. The nonzero steady state probability flux measures the extent of the system from the equilibrium and become nonequilibrium. In the context of reaching a steady state, the divergence of the probability flux is zero ($\nabla \cdot \boldsymbol{J} = 0$), and two scenarios can occur. The first scenario is when $\boldsymbol{J}$ is zero, indicating no net flux, and the system is in a state of detailed balance. The second scenario is when $\boldsymbol{J}$ is nonzero, signifying the breakdown of detailed balance and the presence of a net flux. In this case, the flux is curl or rotational and forms a spiral field. The emergence of flux indicates that open systems exchange matter, energy, or information with the environment. The potential landscape is defined as the negative logarithm of the steady-state probability distribution analogous to Boltzmann's law. Mathematically, it is represented as $U = -\ln P_{ss}$ [22], P_{ss} denotes the probability distribution of the system in the steady state. The potential landscape plays a crucial role in this framework. It provides valuable information about the dynamics and behavior of the system and serves as a measure of the global properties and stability of the system. The driving force of the system can be decomposed into two components: $\boldsymbol{F} = -D\nabla U + \frac{\boldsymbol{J}_{ss}}{P_{ss}}$. The first term on the right-hand side represents the gradient force, while the second term represents the curl force. This decomposition of the force distinguishes between equilibrium and nonequilibrium dynamics. The nonequilibrium dynamics are primarily governed by the gradient force and the curl force. The gradient force drives the system towards the steady state, while the curl force acts as the source of detailed balance breaking, pushing the system away from the equilibrium. In detailed balanced equilibrium systems, only gradient forces are present, similar to the motion of electrons in an electric field. In nonequilibrium systems, curl forces emerge, similar to electrons moving in an electric and magnetic fields. The war and peace network functions as a dynamic nonequilibrium system, continuously exchanging material, information, and energy with the external environment. The system's dynamics are influenced by both the gradient force and the curl force.

In the nonequilibrium steady state, dissipation is a prominent feature that is closely connected to the rate of entropy generation. By quantifying the rate of entropy generation, we can effectively measure the dissipation within the system [23,24]. Furthermore, the rate of entropy generation serves as an indicator of the system's departure from the equilibrium state, offering thermodynamic insights into its overall behavior. In statistical physics, the entropy of a system is defined as a measure of the microscopic disorder or uncertainty of the system, and its mathematical expression is $S = -\int P(\boldsymbol{x}, t) ln P(\boldsymbol{x}, t) \boldsymbol{dx}$. The rate of change in entropy is $\dot{S} = \int (\boldsymbol{J} \cdot \boldsymbol{D}^{-1} \cdot \boldsymbol{J})/\boldsymbol{P}\boldsymbol{dx} - \int (\boldsymbol{J} \cdot \boldsymbol{D}^{-1} \cdot (\boldsymbol{F} - \nabla \cdot \boldsymbol{D}))\boldsymbol{dx}$. The total entropy of the system is the system entropy plus the environmental entropy, where the first term $\int (\boldsymbol{J} \cdot \boldsymbol{D}^{-1} \cdot \boldsymbol{J})/\boldsymbol{P}\boldsymbol{dx}$ indicates the rate of entropy generation, which represents the rate of change of the total entropy. The second term $\int (\boldsymbol{J} \cdot \boldsymbol{D}^{-1} \cdot (\boldsymbol{F} - \nabla \cdot \boldsymbol{D}))\boldsymbol{dx}$ represents the average heat dissipation rate, the entropy change rate or heat dissipation rate exchanged with the environment. The above equation is commonly abbreviated as $\dot{S}_{\text{tot}} = \dot{S} + \dot{S}_{\text{env}}$, the first law of nonequilibrium thermodynamics is thus given, and the total entropy generation is always greater or equal to 0, which gives the second law of nonequilibrium thermodynamics [23]. When the system reaches a steady state, the rate of entropy change within the system becomes 0. At this stage, the total entropy change of the system, including both the system and its environment, is equivalent to the dissipated heat from the environment [22,25–27]. As evident from the equation

mentioned above, the dissipation is directly associated with the rotational flux.

B. Barrier height, transient time

The mean first pass time (MFPT) can describe the stability of the attractor states, which reflects the dynamic timescale of the system from one stable attractor to another. For a critical transition such as saddle node bifurcation, as the system approaches a critical point, the height of the potential barrier between the bistable states becomes smaller. When one state is close to disappearing, the time it takes for the system to escape from one state and transition to another becomes very short, resulting in a higher frequency of transitions. In other words, as the system approaches a critical threshold, the dynamics become more sensitive to small perturbations, and the system can rapidly switch between different states. This phenomenon is often observed in the systems exhibiting dynamical critical transitions such as saddle node bifurcation. The height of the barrier and the corresponding escape time are important factors in understanding the stability and dynamics of the system. By studying the MFPT and the characteristics of the barrier, we can gain insight into the transition dynamics and the likelihood of the system moving from one state to another.

C. Optimal path of nonequilibrium dynamics

The path integral formulation is a powerful tool commonly used in quantum mechanics, statistical mechanics, and quantum field theory to describe the processes of dynamical systems. Here, due to the nonequilibrium nature of the system, the dynamical path between states do not necessarily pass through the saddle point of the potential landscape. To describe the dynamics of the system's probability from an initial state x_{initial} at $t = 0$ to a final state x_{final} at time t, we can formulate it using the path-integral approach. The path integral allows us to consider all possible paths taken by the system between the initial and final states. Mathematically, the path integral is defined as $P(x_{\text{final}}, t|x_{\text{initial}}, 0) = \int \mathcal{D}x(t)\, e^{-S[x(t)]}$, where $P(x_{\text{final}}, t|x_{\text{initial}}, 0)$ represents the probability of the system switching from the initial state to the final state at time t, $\mathcal{D}x(t)$ represents the sum over all possible paths $x(t)$, and $S[x(t)]$ is the action. The action $S[x(t)]$ is typically defined as the integral of the Lagrangian along the time [28–31]:

$$\int dt \left(\frac{1}{2} \nabla \cdot \mathbf{F}(\mathbf{x}) + \frac{1}{4} \left(\frac{d\mathbf{x}}{dt} - \mathbf{F}(\mathbf{x}) \right) \cdot \frac{1}{\mathbf{D}(\mathbf{x})} \cdot \left(\frac{d\mathbf{x}}{dt} - \mathbf{F}(\mathbf{x}) \right) \right).$$

D. Time-reversal symmetry breaking

The average value of the difference between the forward and backward cross correlation in time of two random time series enables us to evaluate the degree of breaking the detailed balance or nonequilibrium and time irreversibility. The average of the difference between the forward correlation function and backward correlation function in time is defined as

$$\Delta \text{CC} = \sqrt{\frac{1}{t_{\text{f}}} \int_0^{t_f} (C_{XY}(\tau) - C_{YX}(\tau))^2 d\tau}.$$

$C_{XY}(\tau)$ is the forward cross-correlation function in time, and its mathematical expression is as follows: $C_{XY}(\tau) = \langle X(0)Y(\tau) \rangle = \sum X^i Y^j P_i^{ss} P_{ij}(\tau)$. $C_{YX}(\tau)$ is the backward cross-correlation function in time, X and Y represent the time series of two random variables, and τ represents the lag time between the two time series. P_{ij} is the probability from state i to state j at time τ. ΔCC quantifies the behavior of the system and the asymmetry in its dynamics [32,33], and it may also serve as an signal indicator for predicting critical transitions.

E. Critical slowing down

The phenomenon known as critical slowing down often manifests when complex dynamic systems approach a tipping point [34]. Increasing research indicates that critical slowing serves as a precursor signal preceding abrupt changes in complex systems [35–37]. When the external control parameters are altered, the fluctuations in the random sequence become noticeably amplified as the system approaches the critical transition. This amplification occurs due to the decreased elasticity of the stable attractor basin. Additionally, the correlation time of the autocorrelation function for the random variable can show a sharp increase. This inspires us to directly predict the critical points by measuring the stochastic time series. By monitoring and analyzing the fluctuations in the time series data, including their amplitude and correlation properties, one can potentially identify the approaching critical points in complex systems [38]. This approach allows us to gain valuable insights into the dynamics and behavior of the system, enabling us to predict the critical transitions before they appear.

IV. RESULTS AND DISCUSSION

A. Landscape and flux of war and peace network system

In the landscape and flux theory of nonequilibrium systems, the variables U or P capture the system's dynamic behavior within the state space. As mentioned earlier, the steady-state probability distribution holds a crucial role in describing the system's behavior. On the one hand, solving the diffusion Eq. (4) directly is a feasible approach for a small number of variables. However, when confronted with systems that possess more than three dimensions, solving multidimensional partial differential equations becomes increasingly challenging [39]. Alternatively, we can obtain the steady probability distribution function by collecting statistics from the trajectories of all variables in stochastic dynamics simulations. Here, we employ the Heun algorithm for the stochastic dynamics simulation purposes [40].

The global characteristics and dynamic stability of war and peace systems are determined by the underlying landscape. It plays a crucial role in shaping the behavior of the system, influencing its propensity towards war or peace. By analyzing and understanding the landscape, we can gain insights into the overall dynamics and stability of the system. In our stochastic model, we have quantified the landscape and flux, revealing the presence of two attractors in certain parameter regions. These attractors represent stable states in the system and have a significant impact on its behavior and stability. By studying the dynamics and properties of these attractors, we can gain valuable insights into the

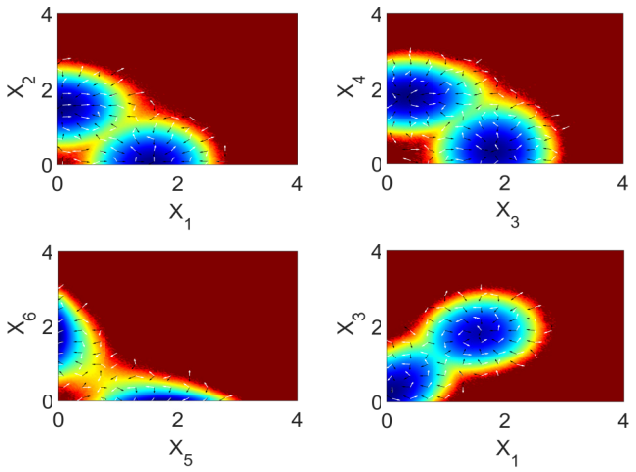

FIG. 3. The two-dimensional projection of the landscape where $D = 0.05$ and $C_{62} = C_{51} = 1.5$, the white arrows represent the flux, and the black arrows represent the force from negative gradient of the landscape.

underlying mechanisms that govern the transition between war and peace, as well as the global stability of the system. These two attractors correspond to distinct states of the system, with one representing the state of peace and the other representing the state of war. The potential landscapes, visualized through the two-dimensional projections, are depicted in Fig. 3. The positions of the war and peace states in the state space are as follows: (0.08, 1.59, 0.3, 1.83, 0.04, 1.75) for the peace state and (1.55, 0.1, 1.83, 0.38, 1.77, 0.04) for the war state. In the state of war, positive factors tend to approach zero, while negative factors exhibit larger positive values. Conversely, in the state of peace, positive factors have higher values and negative factors have lower values. From the figure, it is evident that the gradient force serves to stabilize the peace system within the war attractor basin or the peace attractor basin. In contrast, the curl force acts as a driving force, inducing the movement of the peace system from the war attractor basin to the peace attractor basin or vice versa.

For the purpose of our analysis and discussion, we will focus on the projections in dimensions x_3 and x_4. In our investigation, we discovered that modifying the strength of positive history memory's influence on the positive reciprocity and negative history memory's influence on the negative reciprocity triggers a transition in the system from a monostable state to a bistable state and eventually back to a monostable state. By manipulating these parameters, we can explore the impact of history memory and the resultant reciprocity on the peace system.

In the following discussion, we will record the strength of influence of positive history memory on positive reciprocity as C_{51} and the strength of influence of negative history memory on negative reciprocity as C_{62}.

B. Results under the C_{51} parameter

In Fig. 4(a), the stochastic phase diagram of the system is presented, revealing three distinct regions. It can be observed

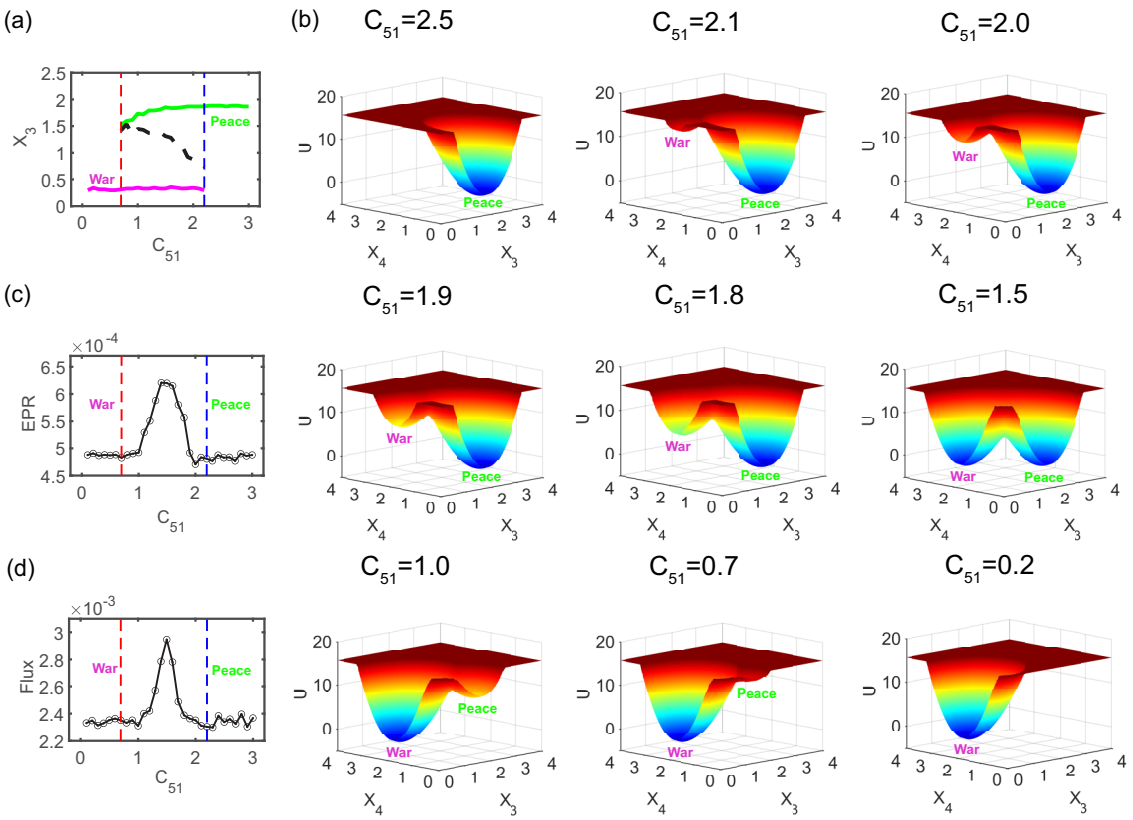

FIG. 4. (a) The stochastic phase diagram for changing the parameter C_{51} with $D = 0.05$. (b) Landscapes versus parameter C_{51}. (c) Rate of entropy production versus parameter C_{51}. (d) Flux versus parameter C_{51}.

that when parameter C_{51} falls within the range of greater than 0.7 and less than 2.2, the system exhibits two states. The green line represents the state of peace, indicating a relatively stable and harmonious condition. The pink line represents the state of war, signifying a state of conflict and hostility. The dashed line in the middle represents the unstable state, where the system is prone to fluctuations and transitions between war and peace. The red and blue dashed lines are used to indicate the war and peace network system approaching the two critical points of war and peace, respectively.

In Fig. 4(b), it can be observed that the topography of the potential landscape undergoes changes as the strength of the influence of positive history memory on positive reciprocity varies. As the parameter strength of the influence of the positive history memory on positive reciprocity decreases, positive history memory reduces, leading to a decrease in positive reciprocity and making the peace state more unstable, facilitating a transition to the state of war. Conversely, as the parameter strength of the influence of the positive history memory on positive reciprocity increases, positive history memory rises, resulting in an increase in positive reciprocity and making the state of war more unstable, facilitating a transition to the state of peace. Please note that we emphasize the impact of history memory on the reciprocity rather than the impact of reciprocity on the history memory. These two aspects are entirely distinct, as shown in Fig. 1, where parameters C_{51} and C_{15} are entirely different. When C_{51} is set to 1.5, the weights of war and peace become equal, indicating a balanced state between the two. However, when the parameter C_{51} deviates significantly from 1.5, either towards smaller or larger values, the system shows a clear dominance of either war or peace. This finding suggests that the strength of influence of the positive history memory on the positive reciprocity plays a crucial role in determining the relative importance of war and peace within the system. By varying the value of C_{51}, we can observe a shift in the system's behavior, indicating the significance of this parameter in shaping the prevalence of war or peace. This emphasizes the system's sensitivity to variations in the strength of the positive reciprocal effects caused by the positive history memory. It underscores the significance of comprehending and examining the impact of this parameter on the dynamics of war and peace.

1. Thermodynamic and dynamical origins of nonequilibrium phase transitions

The EPR is a measure of the thermodynamic cost, while the rotational flux represents the driving force for nonequilibrium processes. As a nonequilibrium system, the war and peace network system interacts with the environment by exchanging various elements such as matter, energy, information, and more. Figure 4(c) illustrates the relationship between the EPR and the strength of influence of the positive history memory on positive reciprocity. It is observed that the EPR reaches a peak around $C_{51} = 1.5$, indicating that when war and peace coexist with similar weights, the system requires more cost to maintain stability.

Figure 4(d) presents the relationship between the average flux and the strength of influence of the positive history memory on positive reciprocity. Remarkably, the trend of the flux aligns with that of the EPR, indicating a close connection between the flux and the cost of the system. Although the landscape gradient tends to stabilize the point attractors, the flux, due to its rotational nature, tends to destabilize the stability of the point attractors.

From Fig. 5, it can be observed that the flux is distributed in a rotating manner around each stable state attractor and also propagates between different stable state attractors. As the strength of positive reciprocity influence from the positive history memory decreases, the flux initially increases and then decreases. This leads to a reduction in the stability of the original state of peace and the emergence of a new war state. Throughout this process, the associated thermodynamic cost also increases, as the creation of the new state requires dissipative cost. As the parameter further decreases, the flux decreases, and a single war attractor becomes preferred, as the decrease in flux and the associated cost destabilize the coexistence of the bistable basins. Therefore, increasing the flux disrupts the stability of the states, while the EPR provides the thermodynamic cost of the instability. As the degree of nonequilibrium in the system increases, more dissipation is required to maintain the stability, resulting in higher EPRs. Thus, in nonequilibrium systems, the flux and EPR work together, revealing the dynamic and thermodynamic mechanisms of stability disruption, thereby promoting the occurrence of phase transitions, bifurcations, and new state formation.

2. Barrier height and early warning indicators

The barrier between the two state basins plays a crucial role in determining the transition time of the system from one state to another. We can quantify the barrier height as $\Delta U = U_{\text{saddle}} - U_{\text{state}}$, which represents the difference between the height of the saddle point and the height of the basin floor on the landscape. The results presented in Fig. 6 are discussed with the peace state as the reference point, which corresponds to the initial position of the stochastic differential Eq. (2). As C_{51} decreases to around 0.7, the positive history memory becomes weaker, resulting in a weaker positive reciprocity. This leads to a decrease in the barrier height. The lower barrier makes it easier for the system to switch from the peace attractor to the war attractor, increasing the likelihood of transitioning towards the war state.

The MFPT is a measure that captures the timescale of the dynamics between stable states, representing the duration needed to switch from one attractor to another. Specifically, it quantifies the time required to move from a region near one attractor to a small vicinity of another attractor. This metric bears significant relevance to the stability of attractor for war and peace. To compute the MFPT, we start by setting the initial conditions of Eq. (2) (Langevin equation) to match the position of the peace state. We then utilize the Heun algorithm to numerically integrate the equation. Simultaneously, we track the trajectory and measure the time it requires for the trajectory to reach a predefined region close to the target attractor (state of war). This entire procedure is repeated 100 times and, finally, the average of the obtained times is calculated to determine the MFPT. As shown in Fig. 6(b),

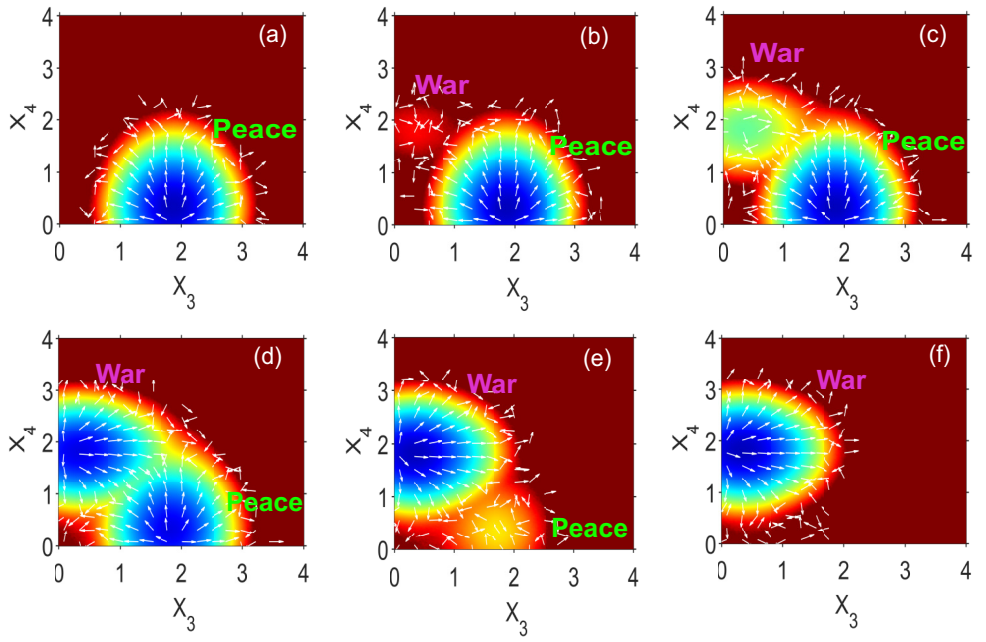

FIG. 5. Nonequilibrium potential landscapes and the curl flux distributions with increasing strength of the influence of the positive history memory on positive reciprocity. The white arrows represent the curl flux on the landscapes ($D = 0.05$). (a) $C_{51} = 2.5$. (b) $C_{51} = 2.1$. (c) $C_{51} = 1.8$. (d) $C_{51} = 1.5$. (e) $C_{51} = 1.0$. (f) $C_{51} = 0.2$.

the MFPT from the peace state to the war state decreases as the strength of influence of the positive history memory on positive reciprocity decreases. The frequency, which is the reciprocal of the MFPT, exhibits a gradual increase as shown in Fig. 6(d). In the vicinity of the war tipping point highlighted by the red dashed line in the figure, the frequency experiences a remarkable surge, which we refer to as the flickering frequency.

In Fig. 6(e), the correlation time of the autocorrelation functions for the stochastic series is shown as a function of the parameters. The phenomenon known as critical slowing down is observed when a system approaches a tipping point. As the system approaches the tipping point of war, the basin depth in the landscape decreases, indicating a reduction in resilience within the state of peace. This implies that the state of peace becomes more unstable, thereby elevating the risk of transitioning to a state of war. Consequently, when the system approaches the critical point, critical slowing-down autocorrelation time(correlation time) experiences a substantial increase.

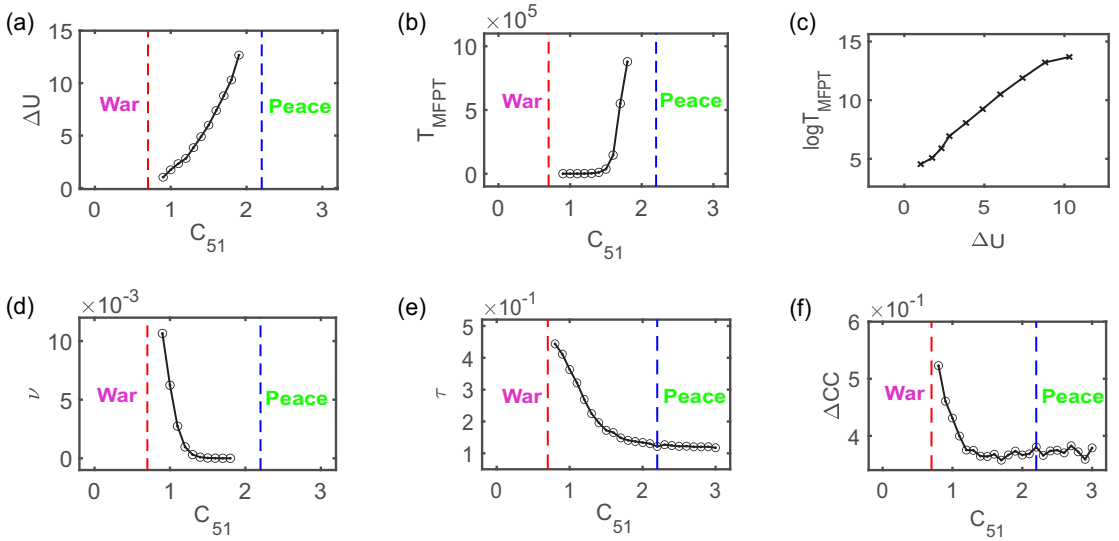

FIG. 6. (a) Barrier height versus parameter C_{51}. (b) Mean first pass time versus parameter C_{51}. (c) Logarithm of mean first pass time parameter C_{51}. (d) Flickering frequency versus parameter C_{51}. (e) Autocorrelation time versus parameter C_{51}. (f) The average of the difference between forward and backward cross-correlation functions versus parameter C_{51}.

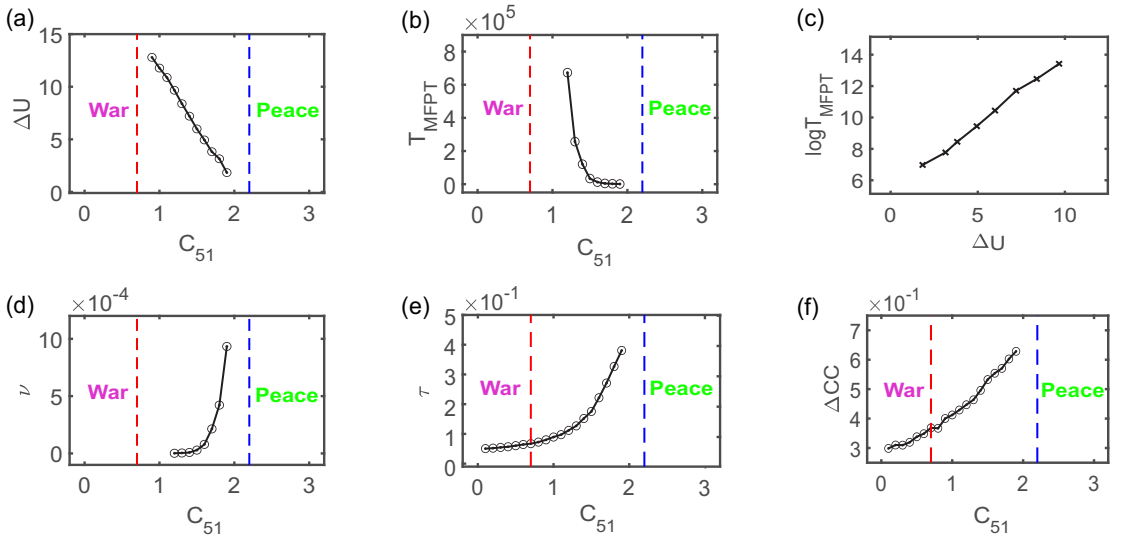

FIG. 7. (a) Barrier height versus parameter C_{51}. (b) Mean first pass time versus parameter C_{51}. (c) Logarithm of mean first pass time parameter C_{51}. (d) Flickering frequency versus parameter C_{51}. (e) Autocorrelation time versus parameter C_{51}. (f) The average of the difference between forward and backward cross-correlation functions versus parameter C_{51}.

Figure 6(f) shows the average of the difference between forward and backward cross correlations in time of the two peace factors (ΔCC) as a function of the parameters. Similar to the flickering frequency and correlation time, it also exhibits a noticeable increase when approaching the war critical point. This observation suggests that it could potentially serve as a predictive indicator for identifying the proximity of the system to a tipping point (more detailed computational information can be found in the Supplemental Material [41]).

In Fig. 7, we show the results with the war state as the reference point, which correspond to the initial position of the stochastic differential Eq. (2). It has been observed that the strength of the influence of the positive history memory on the positive reciprocity increases with the increase of the parameter C_{51}. The state of war became more unstable and the height of the barrier gradually decreased. The MFPT decreases and the corresponding flickering frequency exhibits a sharp increase near the critical point of the peace state, indicated by the blue dashed line in the graph. In addition, it is worth noting that the correlation time and the average difference between forward and backward cross correlations in time of the two peace factors also exhibit a significant increase.

Furthermore, we have discovered a positive correlation between the logarithm of MFPT and the barrier height. This relationship is approximately linear, suggesting that the formula $T_{\mathrm{MFPE}} \sim e^{\Delta U}$ holds true. This observation is shown in Figs. 6(c) and 7(c), and quantitative analysis reveals that the height of the barrier plays a crucial role in determining the timescale of the transitions between war and peace in the system. Specifically, a higher barrier height indicates a greater difficulty in switching to the other state. Thus, the barrier height and escape time serve as the key indicators of the landscape topography and provide quantitative measures of the global stability of the peace network system. The logarithmic relationship between MFPT and barrier height provides insights into the temporal aspects of the state transitions. As the barrier height increases, the system requires more time to overcome the barrier and switch from one state to another. This relationship highlights the role of barriers in shaping the dynamics of the system and underlines their significance in determining the timescales associated with the state transitions. By quantifying the relationship between the MFPT and the barrier height, we gain a deeper understanding of the system's behavior and the influence of the potential barriers on the temporal dynamics of the state transitions.

3. Results under the C_{62} parameter

In contrast to C_{51}, the parameter C_{62} represents the strength of the influence of the negative history memory on the negative reciprocity. The increase of parameter C_{62} signifies a stronger negative history memory, which, in turn, leads to an increase in negative reciprocity. In other words, as the influence of negative history memory becomes stronger, the tendency for negative reciprocal actions or responses also intensifies. Conversely, a decrease in parameter C_{62} indicates a weaker negative history memory, which consequently leads to a weaker negative reciprocity. In simpler terms, as the influence of negative history memory becomes weaker, the likelihood of negative reciprocal actions or responses also diminishes.

4. Thermodynamic and dynamical origins of non-equilibrium phase transitions

Figure 8(a) shows the presence of three distinct states as C_{62} varies; the two critical points in the figure are around 0.7 and 0.2, respectively. The blue dashed line indicates a complete transition to a peace state, while the red dashed line indicates a complete transition to war state. As shown in Fig. 8(b), the landscape topography first switches from a single basin representing peace to two basins and then back to

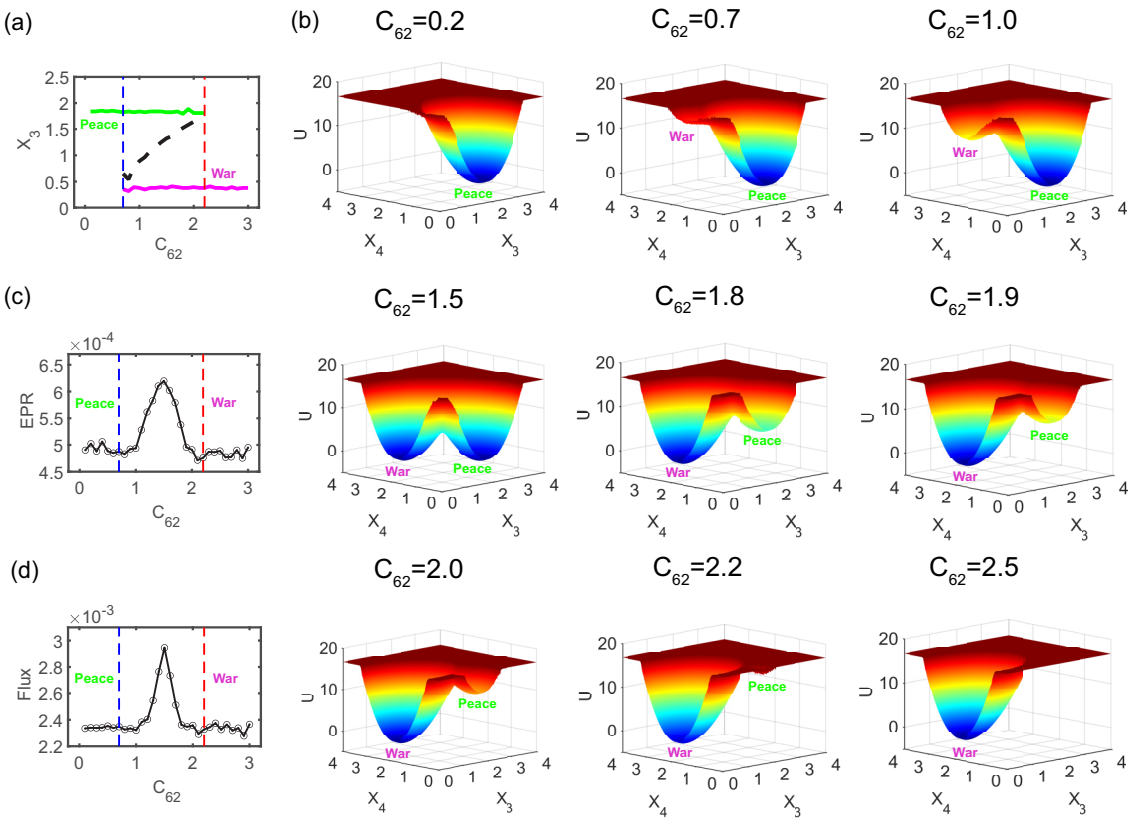

FIG. 8. (a) The stochastic phase diagram for changing the parameter C_{62} with $D = 0.05$. (b) Landscapes versus parameter C_{62}. (c) Rate of entropy production versus parameter C_{62}. (d) Flux versus parameter C_{62}.

a single basin as C_{62} increases. With the gradual attenuation of the impact strength of the negative history memory on the negative reciprocity, represented by the decrease in the parameter C_{62}, the stability of the system's war state is diminished, facilitating a transition towards a state of peace. Conversely, as the impact strength of the negative history memory on the negative reciprocity gradually intensifies, characterized by an increase in the parameter C_{62}, the stability of the system's peace state diminishes, thereby favoring a transition towards a state of war. In Fig. 8(c), we demonstrate the changes in the entropy generation rate as different parameters C_{62} vary. We observe an initial increase followed by a decrease in entropy generation. Furthermore, we find that the weights of the bistable states of peace and war are almost equal when the parameter $C_{62} = 1.5$ and the entropy generation rate reaches its maximum. This indicates that when the negative history memory has a moderate impact on the negative reciprocity, the peace network has the highest degree of imbalance. Notably, maintaining bistability between war and peace incurs higher maintenance costs. Additionally, in Fig. 8(d), we calculate the flux under the influence of the different negative history memories on the negative reciprocity and observe a similar trend to the EPR. Hence, a larger flux corresponds to increased cost.

As shown in Figs. 9, 8(c), and 8(d), due to the distribution of rotational flux, as the influence strength of negative history on the negative reciprocity increases, only one stable peace state appears, and the corresponding dissipation cost is also low. As the influence strength of negative history on the negative reciprocity increases, a bistable coexistence of war and peace gradually emerges, leading to a wider distribution of rotational flux in the state space. The flux propagates between these two stable states, reducing the stability of the original peace state and giving rise to a new state of war with higher thermodynamic dissipation cost. With the continued increase of the influence strength of negative history on the negative reciprocity, the rotational flux between the two states becomes less significant, and the reduction of flux and associated thermodynamic costs disrupt the stability of the bistable basins of war and peace, leading to the war-only state attractor. Therefore, this indicates that the rotational flux provides the dynamic source for driving the bifurcation or nonequilibrium phase transition in the war and peace system, while the EPR provides the thermodynamic cost supply, thus serving as the thermodynamic source for the bifurcation or nonequilibrium phase transition.

5. Barrier height and early warning indicators

In Figs. 10 and 11, we present the computational results with the peace state and the war state as the reference points, respectively. We start by defining the peace state as our reference point. In this context, the initial conditions of Eq. (2) are chosen to correspond to the coordinates of the peace state. As the influence of the negative history memory on the negative reciprocity strengthens, indicated

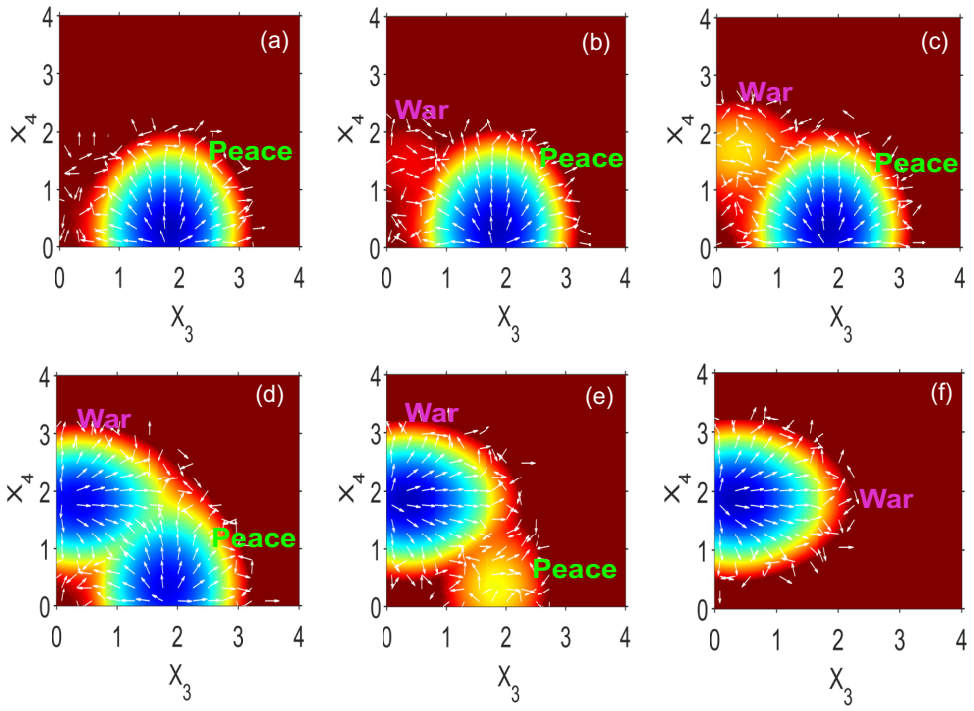

FIG. 9. Nonequilibrium potential landscapes and the curl flux distributions with increasing strength of the influence of the positive history memory on positive reciprocity. The white arrows represent the curl flux on the landscapes ($D = 0.05$). (a) $C_{62} = 0.2$. (b) $C_{62} = 0.7$. (c) $C_{62} = 1.0$. (d) $C_{62} = 1.5$. (e) $C_{62} = 1.9$. (f) $C_{62} = 2.5$.

by an increase in the parameter C_{62}, the risk of switching to a state of war increases. The barrier height, which represents the difficulty in switching between the war and peace states, decreases as C_{62} increases, as shown in Fig. 10(a). This indicates that the system is more prone to switching into a state of war. Figures 10(b) and 10(d) show that when C_{62} approaches 2.2, the MFPT becomes shorter and the flickering frequency increases significantly. Furthermore, Figs. 10(e) and 10(f) demonstrate an increasing trend in the correlation time and the difference in the cross-correlation functions forward in time and backward in time as we approach the critical point on the right (more detailed computational information can be found in the Supplemental Material [41]).

However, if we consider the war state as the reference point, meaning that the initial conditions of Eq. (2) are set to the coordinates of the war state, the situation is reversed. As the influence of the negative history memory on the negative

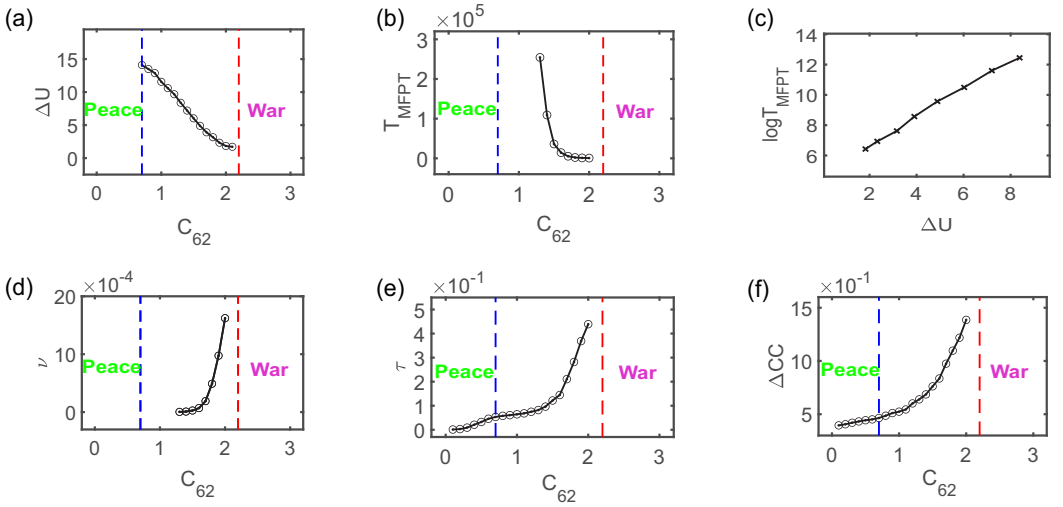

FIG. 10. (a) Barrier height versus parameter C_{62}. (b) Mean first pass time versus parameter C_{62}. (c) Logarithm of mean first pass time parameter C_{26}. (d) Flickering frequency versus parameter C_{62}. (e) Autocorrelation time versus parameter C_{62}. (f) The average of the difference between forward and backward cross-correlation functions versus parameter C_{62}.

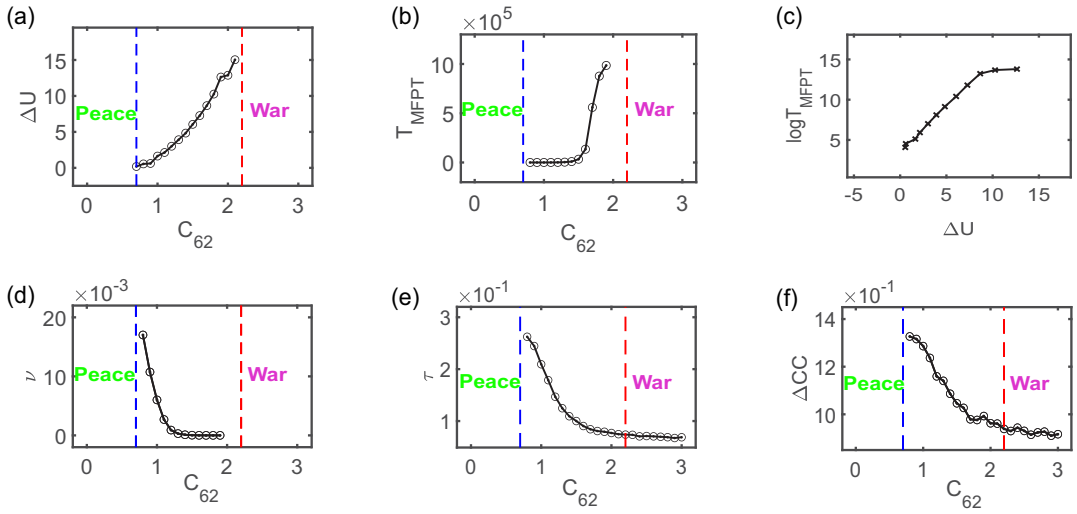

FIG. 11. (a) Barrier height versus parameter C_{62}. (b) Mean first pass time versus parameter C_{62}. (c) Logarithm of mean first pass time parameter C_{62}. (d) Flickering frequency versus parameter C_{62}. (e) Autocorrelation time versus parameter C_{62}. (f) The average of the difference between forward and backward cross-correlation functions versus parameter C_{62}.

reciprocity weakens, indicated by the decrease in parameter C_{62}, the stability of the war state diminishes. Consequently, the likelihood of the system being in a state of war gradually decreases.

When approaching the left critical point, represented by the blue dashed line in Fig. 11, several notable changes occur. The barrier height is lowered, resulting in reduced resistance to transition from a state of war to a state of peace. The MFPT also decreases, indicating a faster transition process. Moreover, there is a sharp increase in the flickering frequency, correlation time, and the average of the difference between forward and backward cross correlations (more detailed computational information can be found in the Supplemental Material [41]). Furthermore, a clear positive correlation between the logarithm of the MFPT and the barrier height can be observed from Figs. 10(c) and 11(c); as previously mentioned, the correlation between the barrier height and the escape time serves as a reliable indicator of stability for war and peace network.

The above analysis highlights the significant impact of history memory on reciprocity within the war and peace network. Stronger positive history memories and a tendency towards positive reciprocity are associated with a higher probability of the system being in a peace state, whereas weaker positive history memories and positive reciprocity tendencies correspond to a higher likelihood of the system being in a state of conflict or war. Conversely, stronger negative history memories and negative reciprocity tendencies increase the likelihood of the system being in a state of war, while weaker negative history memories and negative reciprocity tendencies increase the likelihood of the system being in a state of peace. The influence of history memory on reciprocity has a direct effect on various physical quantities, such as barrier height and MFPT between two states, consequently impacting the system's robustness and stability. Drawing inspiration from the above, using the Ukrainian crisis as an example, if people want to prevent war, they should cultivate positive history memory and consequently reinforce more positive reciprocity. Conversely, when in a state of war, individuals can promote peace by diminishing negative history memory and, in turn, reducing negative reciprocal actions.

C. Comparison of early warning signals

Based on the analysis and discussions above, it is evident that as the system approaches the critical point, there is a significant increase in the flickering frequency, correlation time, and the average difference in cross-correlation functions forward in time and backward in time. This suggests that these three indicators can serve as early warning signals. Therefore, in this paper, we will conduct a comparative analysis to determine which signal predicts the system's state transition earlier.

To analyze the early warning indicators more accurately, we take more data points for parameters C_{62} and C_{51} and calculate three early warning indicators. Figure 12 shows the comparison results when using the peace state and war state as reference points, respectively, under parameter C_{51}. The scatter points in the figure are calculated data, while the solid lines are the results of polynomial fitting. The quantities of the average difference in cross-correlation functions forward in time and backward in time (ΔCC) and critical slowing-down correlation time (CSD) are plotted through the left y axis, while the flickering frequency ν is plotted via the right y axis, indicated by the green color. Taking the peace state as the reference point, as shown in Figs. 12(a) and 12(c), it can be seen that when the system approaches the war critical point, the red dashed line on the left, the significant rise in CSD appears earlier than that of ΔCC, and the significant rise in ΔCC appears earlier than that of the flickering frequency ν. When the war state is taken as the reference point, as shown in Figs. 12(b) and 12(d), as the system approaches the peace critical point, the blue dashed line on the right, the significant rise in ΔCC appears earlier than that of CSD, and the significant rise in CSD appears earlier than that of the flickering

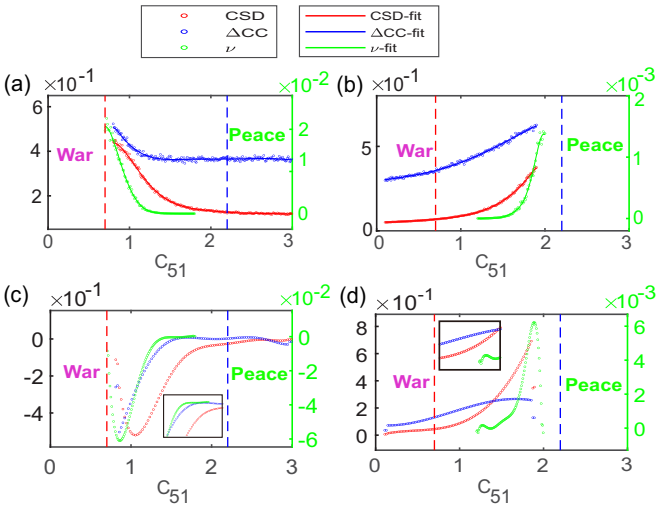

FIG. 12. (a) Comparison figure of three early warning indicators with peace state as reference point under parameter C_{51}. (b) Comparison figure of three early warning indicators with war state as reference point. (c) The derivative image of the fitted image in (a). (d) The derivative image of the fitted image in (b).

frequency ν. In Fig. 13, we show the analysis results under parameter C_{62}. Taking the peace state as the reference point, as shown in Figs. 13(a) and 13(c), it can be seen that when the system approaches the war critical point, the red dashed line on the right, the significant rise in ΔCC appears earlier than that of CSD, and the significant rise in CSD appears earlier than that of the flickering frequency ν. When the war state is taken as the reference point, as shown in Figs. 13(b) and 13(d), as the system approaches the blue dashed line on the left side of the peace critical point, the significant rise in ΔCC emerges earlier than that of the CSD, and the significant rise in CSD appears earlier than that of the flickering frequency ν.

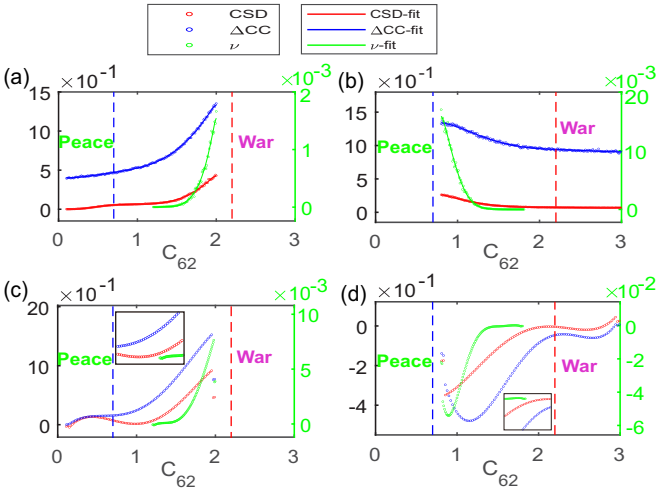

FIG. 13. (a) Comparison figure of three early warning indicators with peace state as reference point under parameter C_{62}. (b) Comparison figure of three early warning indicators with war state as reference point. (c) The derivative image of the fitted image in (a). (d) The derivative image of the fitted image in (b).

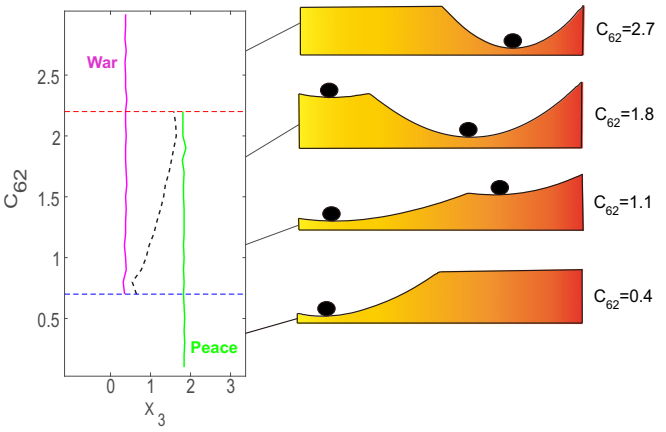

FIG. 14. Stochastic phase diagram and the effective one-dimensional landscapes for different parameters C_{62}, where diffusion coefficient $D = 0.05$.

Based on the above discussion, it can be concluded that, in general, signal index of average difference in cross-correlation functions between forward in time and backward in time often tends to occur earlier than the critical slowing-down index, while the critical slowing-down index often tends to occur earlier than the flickering frequency warning indicator. It is not difficult to understand why these three quantities all exhibit a significant increase approaching the critical point. Taking the parameter C_{62} as an example, we plotted the effective one-dimensional landscape as C_{62} varies as shown in the Fig. 14. It can be seen from Figs. 8(c), 8(d), and 14, when the parameter is small, peace state is preferred. As C_{62} increases, the flux increases. This leads to less stability of the original peace state and the emergence of the new state war. During this process, the associated thermodynamic cost also increases as creating new state wars requires dissipation cost. As the parameter increases further, flux decreases, and a single attractor of war is preferred since the drops of flux and associated cost make the coexistence bistable basins less stable. On the one hand, the sharp increase trend observed near the war critical transition point in ΔCC echoes the essence of flux and EPR, as it reflects the irreversibility or nonequilibrium nature of time. On the other hand, as shown in Fig. 14, with the gradual increase of C_{62}, the basin of the peace state becomes almost flat. Therefore, when perturbed away from the center of the basin, the relaxation back tends to be slow, leading to critical slowing down phenomenon. The flickering frequency of switching from the peace state to the war state increases. The flux and EPR are not easy for the probe to directly detect from the observed time series. However, critical slowing down, flickering frequency, and the ΔCC (time irreversibility) can be obtained directly from the observed time series by calculating autocorrelation and cross-correlation functions. Therefore, they can serve as early warning indicators for predicting the emergence of war.

D. Optimal path of nonequilibrium dynamics

We quantified the dominant paths between the war and peace basins of attraction and utilized Monte Carlo methods to minimize the action and identify the major paths [16,28,42].

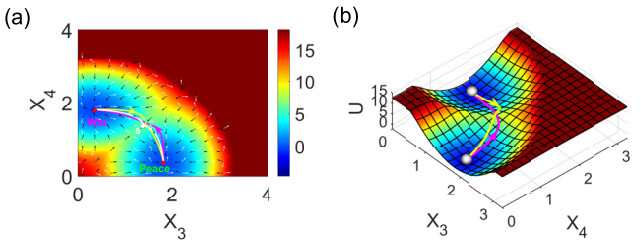

FIG. 15. (a) Two-dimensional optimal path, where $D = 0.05$ and $C_{62} = C_{51} = 1.5$. The pink line represents the path from peace to war, the yellow line represents the path from war to peace. (b) Three-dimensional optimal path which is the path in three-dimensional space.

Figure 15(a) shows the two-dimensional dominant paths. The white line segment represents the reversible path solely driven by gradient force, while the yellow and pink lines depict the optimal paths from war to peace and from peace to war, respectively. The presence of rotational flux causes the dominant transition paths of the system to deviate from the steepest path on the landscape, bypassing the saddle point. Therefore, the difference in forward and backward dominant paths reflects the role of the rotational flux force and the degree of the time irrerersibility. Figure 15(b) shows the three-dimensional dominant path.

E. Global sensitivity analysis

To determine the key parameters governing the interaction strengths between two variables influencing the peace in the peace and war network, we conducted a global sensitivity analysis of the interaction strengths for all peace factors. We defined the difference in potential between a saddle point on the landscape and a steady-state attractor as the barrier height, which quantifies the ability to transition between different attractor basins. As depicted in Fig. 16, we increased the intensity of all interactions in the model by 10%, resulting in corresponding changes in the barriers. Subsequently, we calculated the changes in barrier height specifically for the war state. The findings revealed that the alterations in the influence strength of the positive history memory on the positive reciprocity and the negative history memory on the negative reciprocity had the most significant impact on the barrier height. A greater disparity in the change values of the barriers indicates that the influence of history memory on reciprocity plays a major role in the transition between the bistable states of war and peace; the results align with our everyday experiences.

V. CONCLUSION

In this paper, we utilized the framework of landscape and flux theory to quantitatively and comprehensively elucidate the underlying physical processes governing the nonequilibrium dynamics of war and peace. War and peace have been described as two attraction basins, and the dynamics of war and peace network systems determined by both gradient force and curl flux force. The gradient force stabilizes the system in either a state of peace or a state of war, while the curl flux

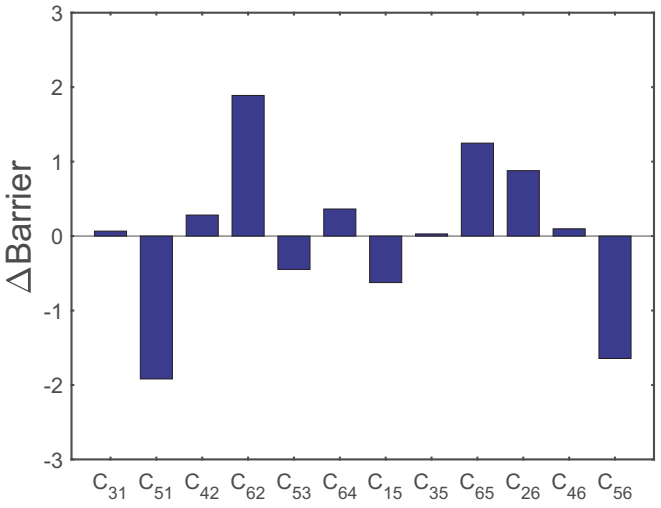

FIG. 16. Global sensitivity analysis for the strength of interaction of various peace factors with $D = 0.05$. The x-axis represents the 12 impact strength of interaction among peace factors. The y-axis represents the barrier changes. When each parameter is individually increased by 10%, the barrier of the state of war changes.

force propels the system away from the steady-state attractor providing the dynamical origin of the bifurcation and early warning signal for the associated critical transition.

EPR and curl flux are intimately related, serving as metrics to quantify the extent to which the peace network system deviates from equilibrium. A higher EPR and stronger flux imply a greater cost. In addition, EPR serves as the thermodynamic origin or nonequilibrium phase transition of the bifurcation, providing a prediction of the tipping point between war and peace.

We calculated the barrier between the basins of war and peace, which determines the duration required to switch from war to peace or from peace to war. The height of the barrier and the MFPT can be utilized to quantify the global stability of the nonequilibrium war and peace network. When the interaction parameters change, it will directly affect the barrier height between the war and peace attraction basin, thus influencing the transition time of the two states. Furthermore, our findings indicate that a stronger influence of the positive history memory on the positive reciprocity leads to a higher tendency towards a state of peace. Conversely, when the influence of the negative history memory on the negative reciprocity is stronger, the system is more prone to a state of war. Thus, fostering a more positive history memory and promoting increased positive reciprocity would be more effective for avoiding prolonged states of war and favoring a state of peace.

Although rotational flux and EPR can be used as dynamical sources of bifurcation or nonequilibrium phase transition points and provide predictable means, they are not easily obtained experimentally, whereas flickering frequency, critical slowdown, and the average of the difference in cross correlations between forward and backward in time (time irreversibility) are easily measured from the time series directly and give predictions. We find the flickering frequency, critical slowing-down correlation time, and the average of the

difference between forward and backward cross correlations increase sharply approaching the critical point (bifurcation point or nonequilibrium phase transition point). These three indicators can be used as early warning indices for the critical transitions. In most cases, we observed that the significant rise in average of the difference between forward and backward cross correlations or the time irreversibility often occurs before that of the critical slowing-down autocorrelation time, with the significant rise in the flickering frequency being the latest to occur.

The presence of the rotational flux as a nonequilibrium driving force results in an irreversible dominant pathway between war and peace, bypassing the landscape saddle points.

Through a global sensitivity analysis of the barrier height, we find that the strength of the influence of history memory on reciprocity emerges as a key factor influencing the dynamics of war and peace. This echoes the dynamic phase transition behavior similar to saddle node bifurcation when we change parameters C_{51} and C_{62}.

In summary, our paper has delved into the dynamics of the war and peace network from a nonequilibrium perspective, providing valuable insights into the complex nature of war and peace. Our paper also provides a quantitative and physical description of the dynamics of war and peace and offers a practical approach for accurately predicting critical points (bifurcation points or nonequilibrium) of war and peace transitions. The framework of landscape and flux theory that we propose is universal and can be applied to other complex networks or systems in the field of sociology.

ACKNOWLEDGMENTS

L.Q.W. and K.Z. thank support from grant the National Natural Science Foundation of China Grant No. 21721003. No. 12234019. L.Q.W. and K.Z. thank useful discussions from L. Xu, L. Zhu, X. Wang, Y. Wu and W. Li.

[1] P. F. Diehl, Exploring peace: Looking beyond war and negative peace, Int.l Stud. Q. **60**, 1 (2016).

[2] L. S. Liebovitch, P. R. Peluso, M. D. Norman, J. Su, and J. M. Gottman, Mathematical model of the dynamics of psychotherapy, Cognit. Neurodyn. **5**, 265 (2011).

[3] L. S. Liebovitch, V. Naudot, R. Vallacher, A. Nowak, L. Bui-Wrzosinska, and P. Coleman, Dynamics of two-actor cooperation- competition conflict models, Physica A **387**, 6360 (2008).

[4] J. M. Gottman, J. D. Murray, C. C. Swanson, R. Tyson, and K. R. Swanson, *The Mathematics of Marriage*, Dynamic Nonlinear Models (Bradford Books, MIT Press, Cambridge, Massachusetts, London, England, 2005).

[5] P. T. Coleman, R. R. Vallacher, A. Nowak, and L. Bui-Wrzosinska, Intractable conflict as an attractor: A dynamical systems approach to conflict escalation and intractability, Am. Behav. Sci. **50**, 1454 (2007).

[6] J. P. Lederach, *Sustainable Reconciliation in Divided Societies* (USIP, Washington, DC, 1997).

[7] R. Jervis, *System Effects: Complexity in Political and Social Life* (Princeton University Press, Princeton, 1998).

[8] M. Deutsch, P. T. Coleman, and E. C. Marcus, *The Handbook of Conflict Resolution: Theory and Practice* (Jossey-Bass, San Francisco, 2006).

[9] M. E. J. Newman, The structure and function of complex networks, SIAM Rev. **45**, 167 (2003).

[10] P. T. Coleman, L. S. Liebovitch, and J. Fisher, Taking complex systems seriously: Visualizing and modeling the dynamics of sustainable peace, Global Policy **10**, 84 (2019).

[11] L. S. Liebovitch, P. T. Coleman, B. Fisher-Yoshida, J. Fisher, K. Mazzaro, D. Fry, P. Vandenbroeck, and S. Ortiz, Challenge problem: Sustainable peace, Bloomberg Data for Good Exchange Conference, September 2015.

[12] L. S. Liebovitch, P. T. Coleman, D. Futran, D. Lee, T. Lichter, N. Burgess, D. Maksumov, and C. C. Ripla, Modeling the dynamics of sustainable peace, in *Mathematical Modeling of Social Relationships: What Mathematics Can Tell Us About People* (Springer, Cham, 2018), pp. 147–159.

[13] L. S. Liebovitch, P. T. Coleman, A. Bechhofer, C. Colon, J. Donahue, C. Eisenbach, L. Guzmán-Vargas, D. Jacobs, A. Khan, C. Li *et al.*, Complexity analysis of sustainable peace: mathematical models and data science measurements, New J. Phys. **21**, 073022 (2019).

[14] P. S. Swain, M. B. Elowitz, and E. D. Siggia, Intrinsic and extrinsic contributions to stochasticity in gene expression, Proc. Natl. Acad. Sci. **99**, 12795 (2002).

[15] J. Wang, Landscape and flux theory of non-equilibrium dynamical systems with application to biology, Adv. Phys. **64**, 1 (2015).

[16] X. Fang, K. Kruse, T. Lu, and J. Wang, Nonequilibrium physics in biology, Rev. Mod. Phys. **91**, 045004 (2019).

[17] P. T. Coleman, J. Fisher, D. P. Fry, L. S. Liebovitch, A. Chen-Carrel, and G. Souillac, How to live in peace? Mapping the science of sustaining peace: A progress report, Am. Phys. **76**, 1113 (2021).

[18] L. S. Liebovitch, P. T. Coleman, and J. Fisher, Approaches to understanding sustainable peace: Qualitative causal loop diagrams and quantitative mathematical models, Am. Behav. Sci. **64**, 123 (2020).

[19] Nicolaas Godfried Van Kampen, *Stochastic Processes in Physics and Chemistry* (Elsevier, Amsterdam, 2007).

[20] C. W. Gardiner, *Springer Complexity: Handbook of Stochastic Methods for Physics, Chemistry and the Natural Sciences* (Springer, Berlin, 2004).

[21] H. Risken, *Fokker-Planck Equation* (Springer, Berlin, 1996).

[22] J. Wang, L. Xu, and E. Wang, Potential landscape and flux framework of nonequilibrium networks: Robustness, dissipation, and coherence of biochemical oscillations, Proc. Natl. Acad. Sci. USA **105**, 12271 (2008).

[23] H. Feng and J. Wang, Potential and flux decomposition for dynamical systems and non-equilibrium thermodynamics: Curvature, gauge field, and generalized fluctuation-dissipation theorem, J. Chem. Phys. **135**, 234511 (2011).

[24] H. Qian, Mesoscopic nonequilibrium thermodynamics of single macromolecules and dynamic entropy-energy compensation, Phys. Rev. E **65**, 016102 (2001).

[25] H. Qian, Open-system nonequilibrium steady state: Statistical thermodynamics, fluctuations, and chemical oscillations, J. Phys. Chem. B **110**, 15063 (2006).

[26] H. Ge and H. Qian, Physical origins of entropy production, free energy dissipation, and their mathematical representations, Phys. Rev. E **81**, 051133 (2010).

[27] F. Zhang, L. Xu, K. Zhang, E. Wang, and J. Wang, The potential and flux landscape theory of evolution, J. Chem. Phys. **137**, 065102 (2012).

[28] J. Wang, K. Zhang, and E. Wang, Kinetic paths, time scale, and underlying landscapes: A path integral framework to study global natures of nonequilibrium systems and networks, J. Chem. Phys. **133**, 125103 (2010).

[29] L. Xu, F. Zhang, K. Zhang, E. Wang, and J. Wang, The potential and flux landscape theory of ecology, PLOS ONE **9**, e86746 (2014).

[30] L. Xu and J. Wang, Landscape and flux for quantifying global stability and dynamics of game theory, PLOS ONE **13**, e0201130 (2018).

[31] J. Wang, K. Zhang, L. Xu, and E. Wang, Quantifying the Waddington landscape and biological paths for development and differentiation, Proc. Natl. Acad. Sci. USA **108**, 8257 (2011).

[32] H. Qian and E. L. Elson, Fluorescence correlation spectroscopy with high order and dual-color correlation to probe nonequilibrium steady states, Proc. Natl. Acad. Sci. USA **101**, 2828 (2004).

[33] L. Xu and J. Wang, Curl flux as a dynamical origin of the bifurcations/phase transitions of nonequilibrium systems: Cell fate decision making, J. Phys. Chem. B **124**, 2549 (2020).

[34] M. Scheffer, *Critical Transitions in Nature and Society* (Princeton University Press, Princeton, 2020).

[35] M. Scheffer, J. Bascompte, W. A. Brock, V. Brovkin, S. R. Carpenter, V. Dakos, H. Held, E. H. Van Nes, M. Rietkerk, and G. Sugihara, Early-warning signals for critical transitions, Nature (London) **461**, 53 (2009).

[36] A. J. Veraart, E. J. Faassen, V. Dakos, E. H. van Nes, M. Lürling, and M. Scheffer, Recovery rates reflect distance to a tipping point in a living system, Nature (London) **481**, 357 (2012).

[37] L. Xu, D. Patterson, S. A. Levin, and J. Wang, Non-equilibrium early-warning signals for critical transitions in ecological systems, Proc. Natl. Acad. Sci. USA **120**, e2218663120 (2023).

[38] V. Dakos, S. R. Carpenter, W. A. Brock, A. M. Ellison, V. Guttal, A. R. Ives, S. Kéfi, V. Livina, D. A. Seekell, E. H. van Nes *et al.*, Methods for detecting early warnings of critical transitions in time series illustrated using simulated ecological data, PloS one **7**, e41010 (2012).

[39] K. Zhang, A. Xia, and J. Wang, The landscape and flux of a minimum network motif, Wu Xing, Chin. Phys. B **29**, 120504 (2020).

[40] R. Toral and P. Colet, *Stochastic Numerical Methods: An Introduction for Students and Scientists* (John Wiley & Sons, Weinheim, 2014).

[41] See Supplemental Material at http://link.aps.org/supplemental/10.1103/PhysRevE.109.034311 for calculations of critical slowing down and time irreversibility. It includes the time trajectories obtained by stochastic dynamics simulation and the autocorrelation and cross-correlation functions calculated by using these time series.

[42] D. C. Khandekar, S. V. Lawande, and K. V. Bhagwat, *Path-Integral Methods and Their Applications* (Allied Publishers, Kolkata, 2002).